Supporting Information: Machine-Learning-Assisted Development and Theoretical Consideration for the $Al_2Fe_3Si_3$ Thermoelectric Material

Zhufeng Hou,[*,†,§] Yoshiki Takagiwa,[*,†,‡,§] Yoshikazu Shinohara,[†,‡] Yibin Xu,[†] and Koji Tsuda[†,¶]

†*Research and Services Division of Materials Data and Integrated System, National Institute for Materials Science, 1-2-1 Sengen, Tsukuba, Ibaraki 305-0047, Japan*

‡*Center for Green Research on Energy and Environmental Materials, National Institute for Materials Science, 1-2-1 Sengen, Tsukuba, Ibaraki 305-0047, Japan*

¶*Graduate School of Frontier Sciences, The University of Tokyo, 5-1-5 Kashiwa-no-ha, Kashiwa 277-8561, Japan*

§*These authors contributed equally to this work.*

E-mail: HOU.Zhufeng@nims.go.jp; TAKAGIWA.Yoshiki@nims.go.jp

1 Structural information of the stable ternary phases in the Al-Fe-Si system

In the established phase equilibria and thermodynamic description of the Al-Fe-Si system, there are eleven stable ternary phases.[S1–S7] They are the $\tau_1(\tau_9)$-$Al_2Fe_3Si_3$, $\tau_2(\gamma)$-Al_3FeSi, τ_3-Al_2FeSi, $\tau_4(\delta)$-Al_3FeSi_2, $\tau_5(\alpha)$-$Al_{7.4}Fe_2Si$, $\tau_6(\beta)$-$Al_{4.5}FeSi$, τ_7-$Al_3Fe_2Si_3$, τ_8-$Al_2Fe_3Si_4$, τ_{10}-$Al_9Fe_4Si_3$, τ_{11}-Al_5Fe_2Si, and τ_{12}-Al_3Fe_2Si phases, where the variant notations are given in brackets if they were used in literature and the nominal formulae are also listed. Only the τ_1, τ_4, τ_7, τ_8, and τ_{12} phases were found to crystallize in the ordered structures,[S7–S10] whose detailed structural information are presented in Table S1.

Table S1: Crystallographic data of the τ_1-$Al_2Fe_3Si_3$, τ_4-Al_3FeSi_2, τ_7-$Al_3Fe_2Si_3$, τ_8-$Al_2Fe_3Si_4$, and τ_{12}-Al_3Fe_2Si phases reported in experiments. The calculated results of the τ_1-$Al_2Fe_3Si_3$ phase by the GGA-PBE method are listed for comparison.

Compound	Space group	Parameters	Experiment[S8–S10]	GGA-PBE
τ_1-$Al_2Fe_3Si_3$	P-1 (2)	a, b, c (Å)	4.684, 6.325, 7.498	4.6032, 6.3256, 7.4594
		α, β, γ (°)	100.99, 105.6, 101.62	101.90, 106.79, 100.59
		Al1, 2i	(0.06814, 0.65441, 0.27676)	(0.05172, 0.64468, 0.27253)
		Al2, 2i	(0.40363, 0.67391, 0.03217)	(0.41424, 0.67513, 0.05218)
		Fe1, 2i	(0.03698, 0.30012, 0.40831)	(0.03990, 0.29241, 0.41558)
		Fe2, 2i	(0.13163, 0.31991, 0.05574)	(0.13515, 0.31778, 0.05655)
		Fe3, 2i	(0.36206, 0.02398, 0.22443)	(0.36468, 0.02816, 0.23271)
		Si1, 2i	(0.28252, 0.05495, 0.54012)	(0.27580, 0.04246, 0.53282)
		Si2, 2i	(0.54301, 0.41573, 0.34732)	(0.54283, 0.41274, 0.34779)
		Si3, 2i	(0.82738, 0.01759, 0.12078)	(0.82049, 0.02395, 0.11363)
τ_4-Al_3FeSi_2	Pbcn (60)	a, b, c (Å)	6.061, 6.061, 9.525	
		Al1, 4a	(0, 0, 0)	
		Al2, 8d	(0.1418, 0.3655, 0.1377)	
		Fe, 4c	(0, 0.0109, 0.25)	
		Si, 8d	(0.3387, 0.1687, 0.3474)	
τ_7-$Al_3Fe_2Si_3$	P21/c (14)	a, b, c (Å)	7.179, 8.354, 15.7076	
		α, β, γ (°)	90, 113.331, 90	
		Al1, 4e	(0.49142, 0.047, 0.16762)	
		Al2, 4e	(0.51102, 0.2039, 0.32282)	
		Al3, 4e	(0.10038, 0.1402, 0.05058)	
		Al4, 4e	(0.10127, 0.6175, 0.05607)	
		Al5, 4e	(0.62249, 0.376, 0.17459)	
		Al6, 4e	(0.07068, 0.3769, 0.27478)	
		Fe1, 4e	(0.17213, 0.11825, 0.22857)	
		Fe2, 4e	(0.17495, 0.63784, 0.23027)	
		Fe3, 4e	(0.29171, 0.62979, 0.53526)	
		Fe4, 4e	(0.29609, 0.37834, 0.03103)	
		Si1, 4e	(0.26441, 0.3748, 0.17331)	
		Si2, 4e	(0.18286, 0.8771, 0.15226)	
		Si3, 4e	(0.16833, 0.6445, 0.37643)	
		Si4, 4e	(0.16826, 0.1138, 0.37396)	
		Si5, 4e	(0.6114, 0.3719, 0.0108)	
		Si6, 4e	(0.3639, 0.379, 0.4672)	
τ_8-$Al_2Fe_3Si_4$	Cmcm (63)	a, b, c (Å)	3.6687, 12.385, 10.147	
		Al, 8f	(0, 0.05746, 0.6086)	
		Fe1, 8f	(0, 0.14896, 0.12537)	
		Fe2, 4c	(0, 0.35285, 0.25)	
		Si1, 8f	(0, 0.31907, 0.015)	
		Si2, 4c	(0, 0.5448, 0.25)	
		Si3, 4c	(0, 0.7396, 0.25)	
τ_{12}-Al_3Fe_2Si	Fd-3m (227)	a, b, c (Å)	10.806, 10.806, 10.806	
		Al, 48f	(0.42756 0.125 0.125)	
		Fe, 32e	(0.21402 0.21402 0.21402)	
		Si, 16c	(0, 0, 0)	

2 Calculated electronic density of states of $Al_2Fe_3Si_3$, $Al_{1.95833}Fe_3Si_3$, $Al_2Fe_3Si_{2.95833}$, $Al_{2.04167}Fe_3Si_{2.95833}$, and $Al_{1.95833}Fe_3Si_{3.04167}$

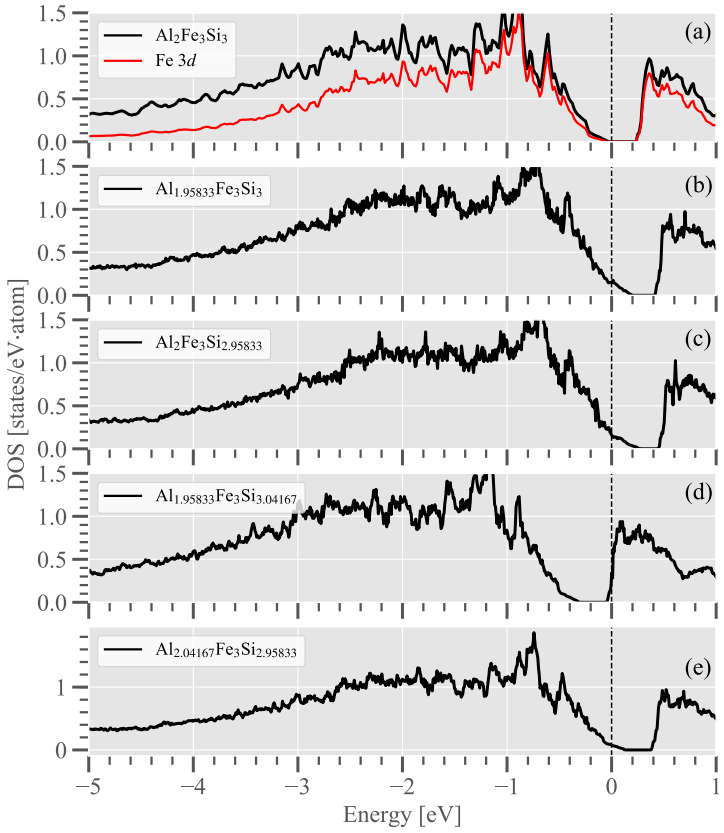

FIG S1: Electronic density of states (DOS) of (a) perfect $Al_2Fe_3Si_3$, (b) $Al_{1.95833}Fe_3Si_3$, (c) $Al_2Fe_3Si_{2.95833}$, (d) $Al_{1.95833}Fe_3Si_{3.04167}$, and (e) $Al_{2.04167}Fe_3Si_{2.95833}$ obtained by the GGA-PBE calculations. The vertical dotted line indicates the position of Fermi level. In panel (a), the averaged DOS of Fe $3d$ orbit is also shown and the position of Fermi level is set to the valence band maximum. The $Al_{1.95833}Fe_3Si_3$, $Al_2Fe_3Si_{2.95833}$, $Al_{1.95833}Fe_3Si_{3.04167}$ and $Al_{2.04167}Fe_3Si_{2.95833}$ were simulated by considering the most stable structures of single Al vacancy, Si vacancy, anti-site substitutional Si for Al, and anti-site substitutional Al for Si in a $3 \times 2 \times 2$ supercell of $Al_2Fe_3Si_3$, respectively.

3 The predicted power factors of $Al_{23.5+x}Fe_{36.5}Si_{40-x}$ ($0.0 \leq x \leq 2.2$ in steps of 0.1) by machine-learning model

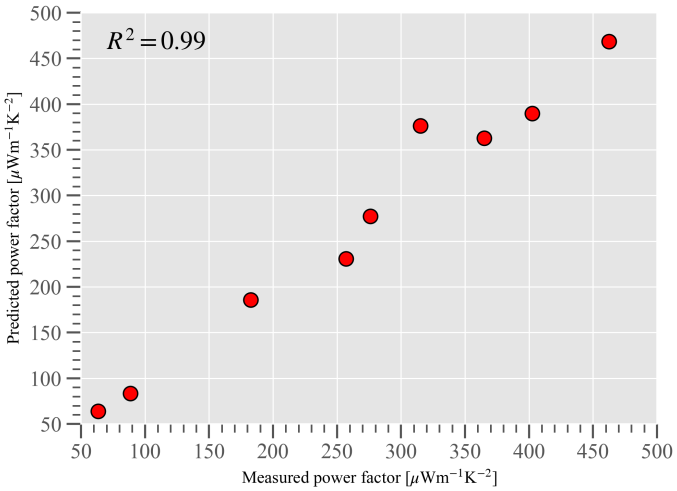

FIG S2: Comparison between the predicted and experimentally-measured power factors for the testing data set, which includes only some of the results of synthesized compositions (x = 0.0, 1.5, 1.8, 2.0, and 2.2). The coefficient of determination (R^2) is about 0.99.

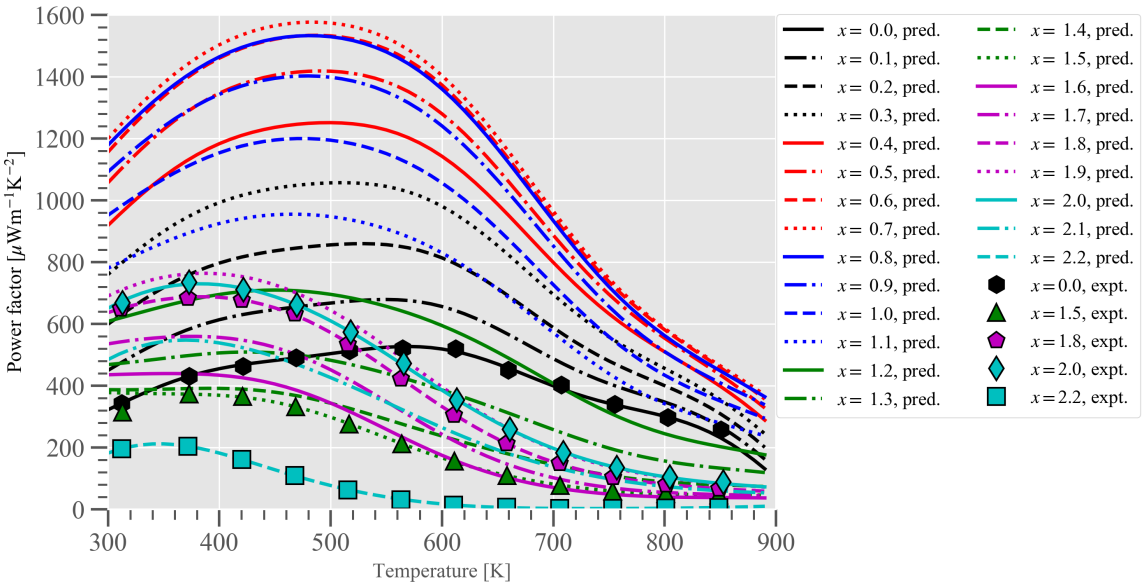

FIG S3: Predicted power factors of $Al_{23.5+x}Fe_{36.5}Si_{40-x}$ by machine-learning model in the first iteration. The experimentally-measured power factors for the synthesized compositions (x = 0.0, 1.5, 1.8, 2.0, and 2.2) are shown for comparison and the corresponding data points are used for building the machine-learning model.

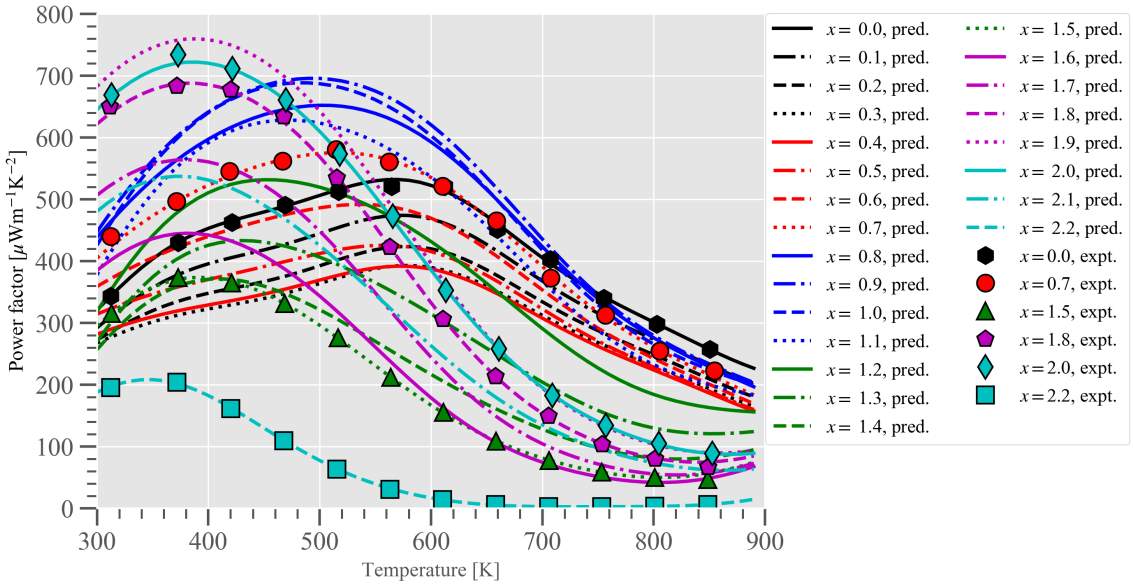

FIG S4: Predicted power factors of $Al_{23.5+x}Fe_{36.5}Si_{40-x}$ by machine-learning model in the second iteration. The experimentally-measured power factors for the synthesized compositions (x = 0.0, 0.7, 1.5, 1.8, 2.0, and 2.2) are shown for comparison and the corresponding data points are used for building the machine-learning model.

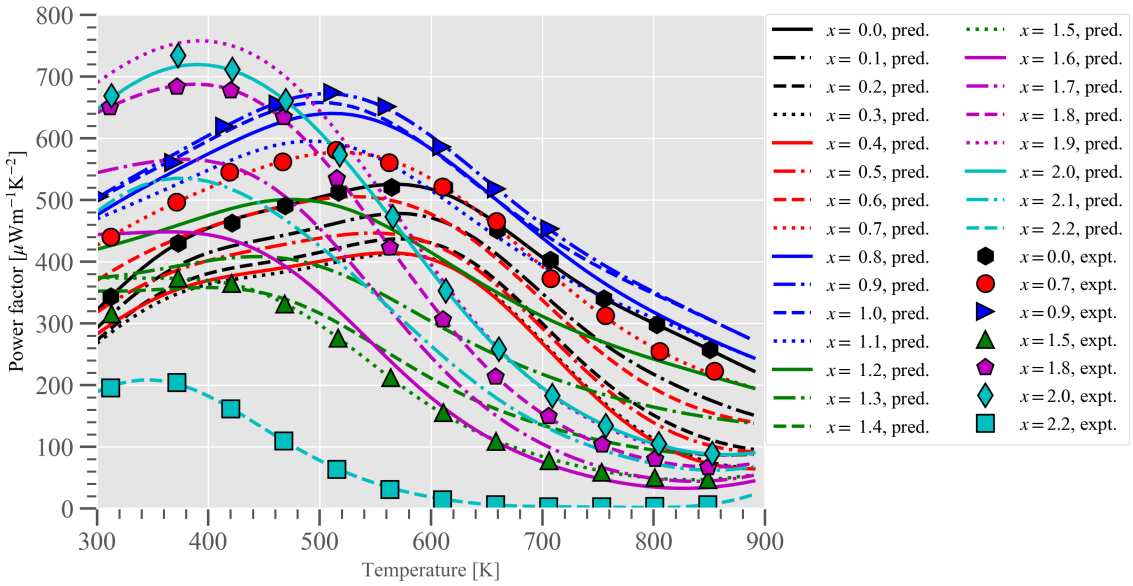

FIG S5: Predicted power factors of $Al_{23.5+x}Fe_{36.5}Si_{40-x}$ by machine-learning model in the third iteration. The experimentally-measured power factors for the synthesized compositions (x = 0.0, 0.7, 0.9, 1.5, 1.8, 2.0, and 2.2) are shown for comparison and the corresponding data points are used for building the machine-learning model.

4 The measured thermoelectric properties of $Al_{23.5+x}Fe_{36.5}Si_{40-x}$, ε-FeSi, and τ_8-$Al_2Fe_3Si_4$

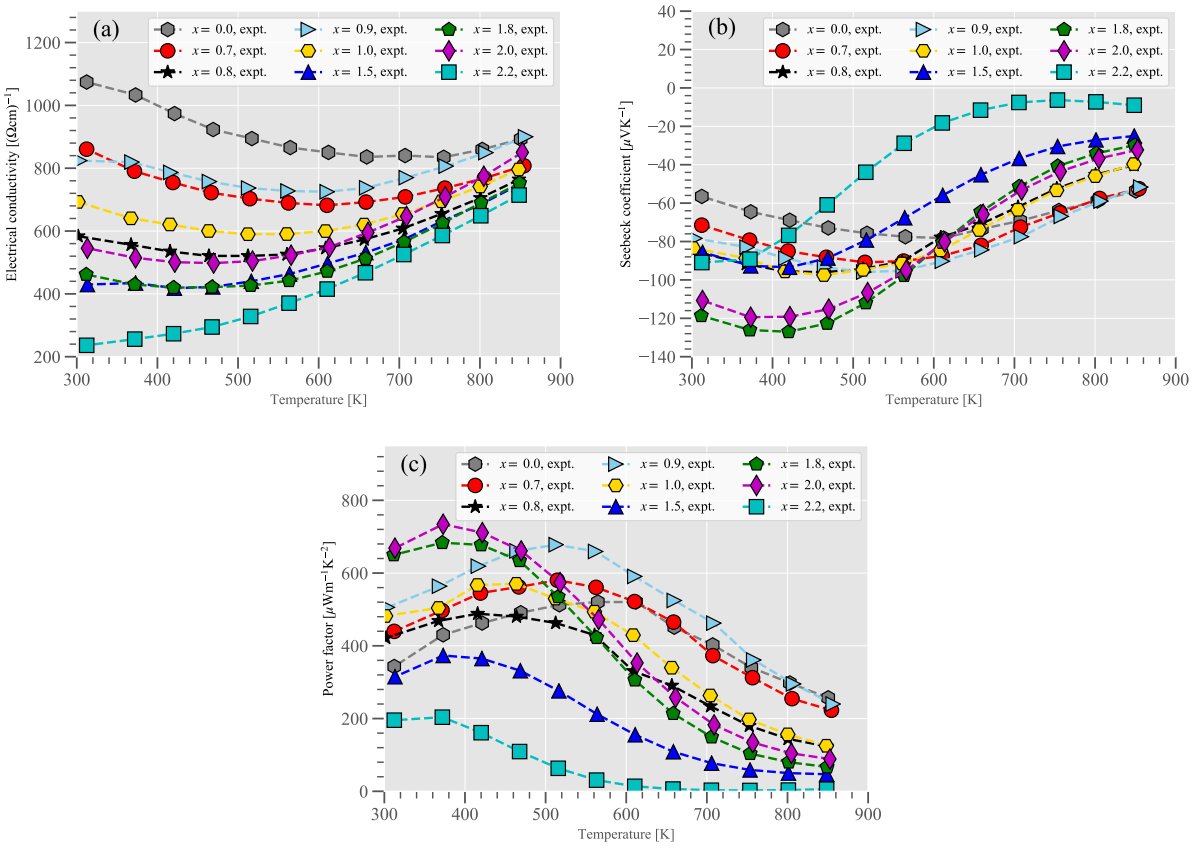

FIG S6: Experimentally-measured (a) electrical conductivity σ, (b) Seebeck coefficient S, and (c) power factor as a function of temperature for $Al_{23.5+x}Fe_{36.5}Si_{40-x}$ at the synthesized compositions ($x = 0.0$, 0.7, 0.8, 0.9, 1.0, 1.5, 1.8, 2.0, and 2.2).

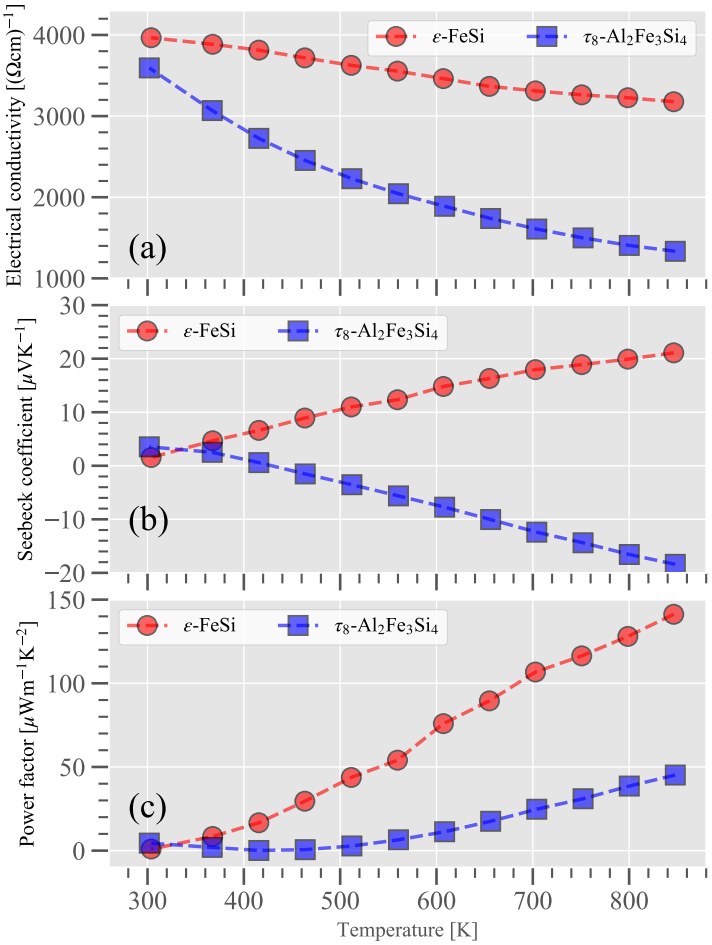

FIG S7: Experimentally-measured (a) electrical conductivity σ, (b) Seebeck coefficient S, and (c) power factor as a function of temperature for ε-FeSi and τ_8-$Al_2Fe_3Si_4$.

5 Calculations of elastic modulus, sound velocity, Debye temperature, and Grüneisen parameter

Because $Al_2Fe_3Si_3$ is a triclinic crystal, 21 independent elastic constants are required to describe its mechanical response. The values of these constants C_{ij} $(i, j = \{1, \ldots, 6\})$ of $Al_2Fe_3Si_3$ are estimated by calculating the stress tensors on applying different deformations to the equilibrium triclinic lattice. The calculated elastic constants are listed in Eq. 1.

$$C_{ij} = \begin{bmatrix} 321.0 & 103.3 & 89.8 & -3.3 & 4.6 & 5.6 \\ & 314.7 & 101.8 & 24.0 & 8.1 & -14.1 \\ & & 335.0 & -1.1 & -1.7 & 9.2 \\ & & & 117.7 & -7.8 & 11.5 \\ & & & & 122.9 & -1.5 \\ & & & & & 126.0 \end{bmatrix} \text{GPa.} \tag{1}$$

From the calculated elastic constants, the macroscopic mechanical parameters such as bulk modulus (B) and shear modulus (G), are calculated using the Voigt (V),[S11] Reuss (R),[S12] and Voigt-Reuss-Hill (H) approaches[S13] in the following forms:

$$B_{\mathrm{V}} = \frac{(C_{11} + C_{22} + C_{33}) + 2(C_{12} + C_{23} + C_{31})}{9} \tag{2}$$

$$B_{\mathrm{R}} = \frac{1}{(s_{11} + s_{22} + s_{33}) + 2(s_{12} + s_{23} + s_{31})} \tag{3}$$

$$G_{\mathrm{V}} = \frac{(C_{11} + C_{22} + C_{33}) - (C_{12} + C_{23} + C_{31}) + 3(C_{44} + C_{55} + C_{66})}{15} \tag{4}$$

$$G_{\mathrm{R}} = \frac{15}{4(s_{11} + s_{22} + s_{33}) - 4(s_{12} + s_{23} + s_{31}) + 3(s_{44} + s_{55} + s_{66})} \tag{5}$$

$$B = \frac{1}{2}(B_{\mathrm{V}} + B_{\mathrm{R}}) \tag{6}$$

$$G = \frac{1}{2}(G_{\mathrm{V}} + G_{\mathrm{R}}) \tag{7}$$

where $s_{ij} = C_{ij}^{-1}$. The Young's modulus (E) and Poisson ratio are evaluated as $E = \frac{9BG}{3B+G}$ and $\nu = \frac{3B-2G}{6B+2G}$, respectively. The calculated bulk modulus, Young's modulus, shear modulus, and Poisson ratio are summarized in Table S2. The obtained elastic modulus of $Al_2Fe_3Si_3$, exceeding 100 GPa, indicate that its mechanical strength could be strong enough for the practical application in thermoelectric device.

Table S2: The bulk modulus (B), Young's modulus (E), shear modulus (G), and Poisson's ratio (ν) of $Al_2Fe_3Si_3$ are calculated according to the Hill averaging scheme and the elastic constants obtained by the GGA-PBE method. The experimental data obtained from the sound velocity measurement of $Al_{23.5+x}Fe_{36.5}Si_{40-x}$ ($x = 0.0$ and $x = 0.9$) in this work and of $Al_2Fe_3Si_3$ in Ref. S14 are also listed for comparison.

	B (GPa)	E (GPa)	G (GPa)	ν
This work	173.1	286.2	116.9	0.224
This work ($x = 0.0$)	131.0	216.3	88.3	0.225
This work ($x = 0.9$)	147.5	237.3	96.3	0.232
Ref. S14	152	249	102	0.226

The propagation velocities of longitudinal (v_{L}) and transverse (v_{T}) acoustic waves are derived from

$$v_{\mathrm{L}} = \sqrt{\frac{E(1-\nu)}{\rho(1+\nu)(1-2\nu)}} = \sqrt{\frac{B+4/3G}{\rho}}, \tag{8}$$

$$v_{\mathrm{T}} = \sqrt{\frac{E}{2\rho(1+\nu)}} = \sqrt{\frac{G}{\rho}}, \tag{9}$$

where ρ is the mass density. The Debye temperature (Θ_{D})[S15] is calculated from the relation

$$\Theta_{\mathrm{D}} = \frac{h}{k_{\mathrm{B}}} \left(\frac{3n}{4\pi\Omega} \right)^{1/3} v_a, \tag{10}$$

where h and k_{B} are Planck and Boltzmann constants, respectively, n is the number of atoms in the cell, Ω is the cell volume, and v_a is the average sound wave velocity. The v_a is given in terms of v_{L} and v_{T} as

$$v_a = \left[\frac{1}{3} \left(\frac{1}{v_{\mathrm{L}}^3} + \frac{2}{v_{\mathrm{T}}^3} \right) \right]^{-1/3}. \tag{11}$$

The Grüneisen parameter γ is calculated from the relation proposed by Belomestnykh:[S16]

$$\gamma = \frac{9 - 12(\frac{v_T}{v_L})^2}{2 + 4(\frac{v_T}{v_L})^2}, \tag{12}$$

which takes into account the contribution of acoustic sound velocities only.

References

(S1) Liu, Z.-K.; Chang, Y. A. Thermodynamic Assessment of the Al-Fe-Si System. *Metall. Mater. Trans. A* **1999**, *30*, 1081–1095.

(S2) Gupta, S. Intermetallic Compound Formation in Fe-Al-Si Ternary System: Part I. *Mater. Charact.* **2002**, *49*, 269–291.

(S3) Maitra, T.; Gupta, S. Intermetallic Compound Formation in Fe-Al-Si Ternary System: Part II. *Mater. Charact.* **2002**, *49*, 293–311.

(S4) Krendelsberger, N.; Weitzer, F.; Schuster, J. C. On the Reaction Scheme and Liquidus Surface in the Ternary System Al-Fe-Si. *Metall. Mater. Trans. A* **2007**, *38*, 1681–1691.

(S5) Du, Y.; Schuster, J. C.; Liu, Z.-K.; Hu, R.; Nash, P.; Sun, W.; Zhang, W.; Wang, J.; Zhang, L.; Tang, C.; Zhu, Z.; Liu, S.; Ouyang, Y.; Zhang, W.; Krendelsberger, N. A Thermodynamic Description of the Al-Fe-Si System over the Whole Composition and Temperature Ranges via a Hybrid Approach of CALPHAD and Key Experiments. *Intermetallics* **2008**, *16*, 554–570.

(S6) Raghavan, V. Al-Fe-Si (Aluminum-Iron-Silicon). *J. Phase. Equilib. Diff.* **2009**, *30*, 184–188.

(S7) Marker, M. C.; Skolyszewska-Kühberger, B.; Effenberger, H. S.; Schmetterer, C.; Richter, K. W. Phase Equilibria and Structural Investigations in the System Al-Fe-Si. *Intermetallics* **2011**, *19*, 1919–1929.

(S8) Gueneau, C.; Servant, C.; d'Yvoire, F.; Rodier, N. $FeAl_3Si_2$. *Acta Cryst. C* **1995**, *51*, 177–179.

(S9) Gueneau, C.; Servant, C.; d'Yvoire, F.; Rodier, N. $Fe_2Al_3Si_3$. *Acta Cryst. C* **1995**, *51*, 2461–2464.

(S10) Yanson, T. I.; Manyako, M. B.; Bodak, O. I.; German, N. V.; Zarechnyuk, O. S.; Cerný, R.; Pacheco, J. V.; Yvon, K. Triclinic $Fe_3Al_2Si_3$ and Orthorhombic $Fe_3Al_2Si_4$ with New Structure Types. *Acta Cryst. C* **1996**, *52*, 2964–2967.

(S11) Voigt, D. W. *Lehrbuch der Kristallphysik*; Taubner: Leipzig, 1928.

(S12) Reuss, A. Berechnung der Fließgrenze von Mischkristallen auf Grund der Plastizitätsbedingung für Einkristalle. *Z. Angew. Math. Mech.* **1929**, *9*, 49–58.

(S13) Hill, R. The Elastic Behaviour of a Crystalline Aggregate. *Proc. Phys. Soc. A* **1952**, *65*, 349.

(S14) Shiota, Y.; Muta, H.; Yamamoto, K.; Ohishi, Y.; Kurosaki, K.; Yamanaka, S. A New Semiconductor $Al_2Fe_3Si_3$ with Complex Crystal Structure. *Intermetallics* **2017**, *89*, 51–56.

(S15) Debye, P. Zur Theorie der spezifischen Wärmen. *Annalen der Physik* **1912**, *344*, 789–839.

(S16) Belomestnykh, V. N. The Acoustical Grüneisen Constants of Solids. *Tech. Phys. Lett.* **2004**, *30*, 91–93.